Prototyping Non-Developable Paper Models without Gluing Tabs

Pok Yin Victor Leung
Massachusetts Institute of Technology
Cambridge, Massachusetts
yck011522@gmail.com

ABSTRACT

The recently revived interest in thin shell architecture demands an efficient method to quickly prototype non-developable surface models for design evaluation. This paper focus on improving the traditional papercraft technique of approximating smooth surfaces with discretised planar meshes. The necessary step to unfold strips of planar faces often creates many separate pieces. These pieces require tedious manual work in gluing and assembling them together. The addition of gluing tabs also results in an aesthetically unpleasing underside of the surface.

This paper proposes a double-shell construction to overcome the challenges of edge jointing and eliminate the need for gluing tabs. A double-shell is created using two sets of unfolded planar strips that were split at different seams. When the two sides are folded and glued back together, the folded connections bridge the seams on another side and vice versa. Spray-on contact adhesive can be globally applied to the underside of each set, thereby speeding up the assembly process.

Models of trimmed and untrimmed NURBS surfaces and triangular mesh surfaces are constructed using this method as demonstration. Quantitative and qualitative effect of model size and paper thickness are explored to provide baseline application parameters. As a result, this method allows anyone with a laser or drag knife cutter to rapidly create mesh models that are easy to assemble and aesthetically clean on both sides.

CCS CONCEPTS

• **Theory of computation → Computational geometry**; • **Computing methodologies → Mesh geometry models**;

KEYWORDS

Digital Fabrication, Rapid Prototyping, Paper Modelling, Papercraft, Weighted-Mesh Representation, Mesh segmentation

ACM Reference Format:
Pok Yin Victor Leung. 2018. Prototyping Non-Developable Paper Models without Gluing Tabs. In *SCF '18: Symposium on Computational Fabrication, June 17–19, 2018, Cambridge, MA, USA.* ACM, New York, NY, USA, Article 4, 11 pages. https://doi.org/10.1145/3213512.3213513

SCF '18, June 17–19, 2018, Cambridge, MA, USA

ACM ISBN 978-1-4503-5854-5/18/06…$15.00
https://doi.org/10.1145/3213512.3213513

1 INTRODUCTION

1.1 Double curved surfaces in architecture

Recent advancement in computational geometry and digital fabrication enabled the construction of expressive double curved architectural surfaces. Double curved geometries can be seen on building facades formed by metal and glass panels, and building structures such as concrete shell and tile vaulted structure [López López et al. 2016].

Early adopters of complex architectural geometry, such as Antoni Gaudi and Frei Otto, designed with physical models [Burry 2016]. Frank Gehry when he designed the Walt Disney Concert Hall, created the forms with physical models before the digitized representation was captured, only for construction rationalization [Stewart 2010]. As human computer interface advanced, contemporary design practice have largely reversed the relationship. Geometries are often modelled digitally as the master copy while physical models are constructed for verification. Yet, the ability to be touched and seen intuitively still offer physical models an important role in the design-evaluation cycle today.

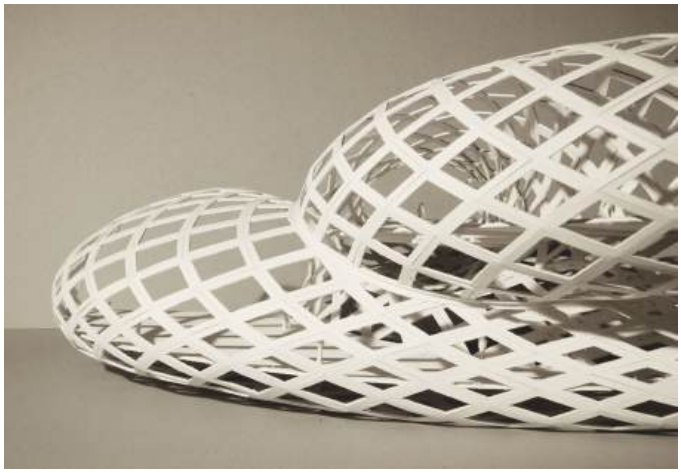

Figure 1: Two intersecting surface constructed with "Double Shell" method.

1.2 Prototyping double curved surfaces

The need for precisely translating digital data into physical models is usually fulfilled by computer controlled fabrication machines such as laser cutters and 3D printers, which are increasingly common in architectural offices. However, these methods are ill suited

for creating non-developable thin shell models. For example, the resolution of 3D printed material dictates the minimum thickness it can achieve. Shapeways 2017 — a 3D printing service company — recommends 0.8mm for their Nylon plastic using Selective Laser Sintering (SLS) and 1.0mm for their PLA plastic using Fused Deposition Modeling (FDM). Curved surfaces also require a disproportionally large amount of support materials under the thin surface, which are slow to print and difficult to remove. The relatively small build volume of 3D printers limits the maximum size of a surface that can be printed without jointing.

On the other hand, laser or drag knife cutters which can efficiently cut flat sheet materials are by definition unable to create non-developable surfaces. One can only join small patches of flat materials to approximate non-developable surfaces. This is similar to the challenge in actual building construction when the desire to create seamless glass facades is limited by the use of flat glass [Lordick 2009]. Recent research have therefore addressed the problem of approximating of smooth surfaces by using patches of developable strips [Elber 1995; Kilian ated; Pottmann and Farin 1995], or together with planar quadrilateral facets [Gonzalez-Quintial et al. 2015; Lordick 2009]. Many smooth surface representations, such as NURBS, can also be discretised into a triangulated mesh and unfolded for fabrication. Pepakura Designer [CORP 2017] a devoted papercraft software, is an example of commercial software that is able to perform mesh segmentation, unfolding and gluing tab generation.

1.3 Face-to-face Connection

While the geometrical problem of approximating smooth surfaces and unfolding meshes are well studied, the manual process of gluing individual faces together is often overlooked. After laser or drag knife cutting, the individual pieces need to be manually folded and glued back together to become a complete model. In order to minimize the number of edges and thus assembly time, complex mesh models can be simplified to low-polygon-count [Garland and Heckbert 1997] or approximated by a smaller set of larger developable strips [Mitani and Suzuki 2004], at the expense of lower resolution.

Individual faces can also be chained into a continuous strip that can be cut together and folded along perforated or engraved lines. The premise of this paper lies on the fact that folding is much easier than gluing, and therefore the careful selection of chains of faces become crucial in reducing manual labour. Various unfolding algorithms exist [Chandra et al. 2015; Mitani and Suzuki 2004] to maximize chain length and minimize chain count. In order to ensure successful unfolding, a self-overlap check is employed during or after the chain selection procedure.

Despite these efforts, a faithful approximation of complex surfaces still requires many separate strips to be fabricated and many edges to be glued. Because it is almost impossible to glue the thin edge between two neighbouring strips, folded tabs are often the solution to provide gluing surfaces. Nevertheless, gluing the tabs requires huge amount of tedious manual work: Glue must be applied uniformly and precisely up to the edge of each tab to avoid oozing or visible gaps; Gluing pressure and alignment need to be maintained while the glue dry in each connection, demanding a lot of time for the assembly. Yet, the finished model is only visually appealing on one side but littered with tabs on the other.

This problem associated with edge gluing is ubiquitous. Folded tabs can be seen in many places from children's folded dice, to some of the physical models created by previously mentioned authors. For example, Chandra et al. [2015] used a half circular gluing tab for their curve-folded mesh; Mitani and Suzuki [2004] even used scotch tape to bridge between strips.

Attempts to solve the edge-to-edge connection had so far been limited. Kilian [2003] demonstrated an edge joining method similar to a 3D jigsaw puzzle. Relying on the friction at the edge of the material, it does not require glue. However, it is not applicable to very thin materials such as paper. Gonzalez-Quintial et al. [2015] used zipper-like edges that appear to be geometrically interlocking without the need of glue. However, the visually distinctive zipper-shaped geometry caused the joints to stand-out from the global surface geometry. That become distracting when the observer is trying to understand the double curved surface model as a whole.

Takezawa et al. [2016] demonstrated a double layer construction approach for freeform surfaces, their method utilize strips extracted along the lines of principle curvature and results in a largely orthogonal pattern. They have also demonstrated a weaving method to construct the surfaces with the extracted strips.

2 PROBLEM

This paper proposes double layer approach to overcome the challenges of edge jointing for prototyping non-developable paper models. The goal is to eliminate gluing tabs and its visual artefacts in the finished model. The difficulty associated with the assembly process is also reduced because contact adhesive can be applied by spraying or rolling.

The method performs best on NURBs surface approximation but can also be generalized for any mesh input. Compared to the algorithm proposed by Takezawa et al. [2016], our method allow user defined mesh tessellation that is not limited to following surface curvature.

3 METHOD

The unrolled version of a non-developable mesh surface will always have edge(s) being separated, and require gluing to reconnect them. The solution proposed in this paper is to generate two sets of strips that have different edge connections, in other words, they are split at different seams. The folded-edge in one of the layers bridge across the cut seams in another layer and vice versa. As long as the folded connections in both layers are combined to complete all necessary connections, no edge gluing is required. It may help to imagine each set of strips as being "one side" of the input mesh surface.

Because each layer of strips is only exposed on one side of the completed surface, the other side can be face-glued to the other set of strips. This arrangement of a clearly defined *exposed side* and a *gluing side* allows global application of spray-on contact adhesive which is substantially faster than individually applying glue to gluing tabs.

Figure 2 shows a comparison between the proposed "Double Shell" method and the traditional "Gluing Tab" method using a

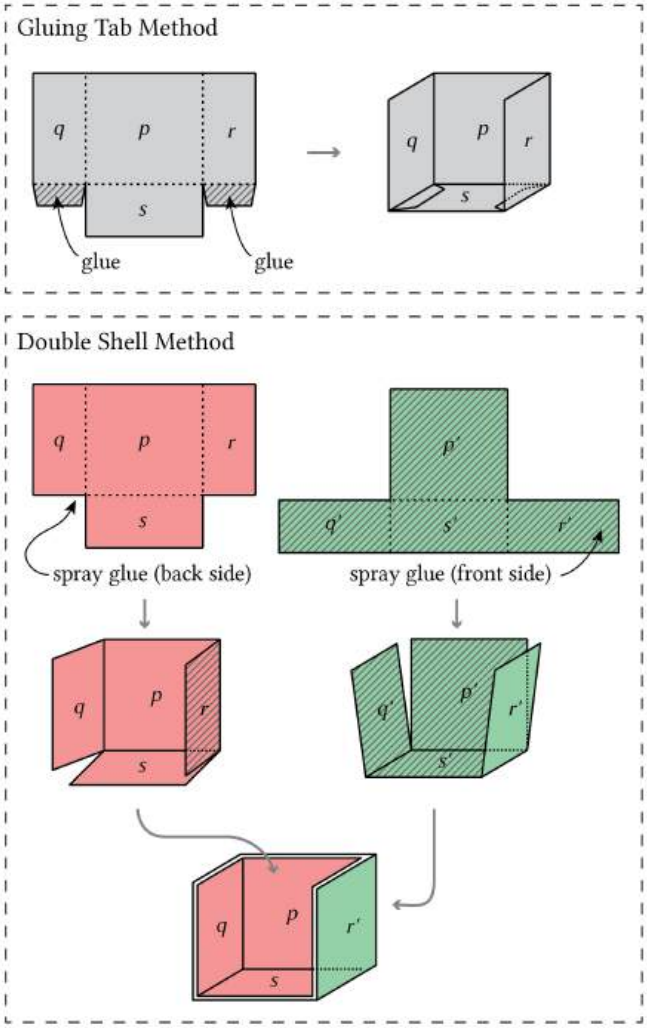

Figure 2: Assembly process of traditional "Gluing Tab" method and the proposed "Double Shell" method.

simplified scenario of a mesh with 4 planar faces and 5 edge connections. In the "Double Shell" method, two strips are unfolded at different seams, they retain the same 4 planar faces but only contains 3 connected edges. The strips can then be fabricated from flat materials, folded and glued together to form the completely connected mesh with all 5 connected edges.

Figure 3 shows a summary of the digital and manual workflow for the "Double Shell" method. Each of the steps will be explained in details in the following text.

3.1 Surface Input

Smooth surface input such as NURBs surface needs to be first converted into a mesh representation that contains only triangles and planar-quads. The tessellation density can be adjusted according to the desired resolution of the approximation. Regular triangular grid pattern is used in the demonstrations presented in this paper.

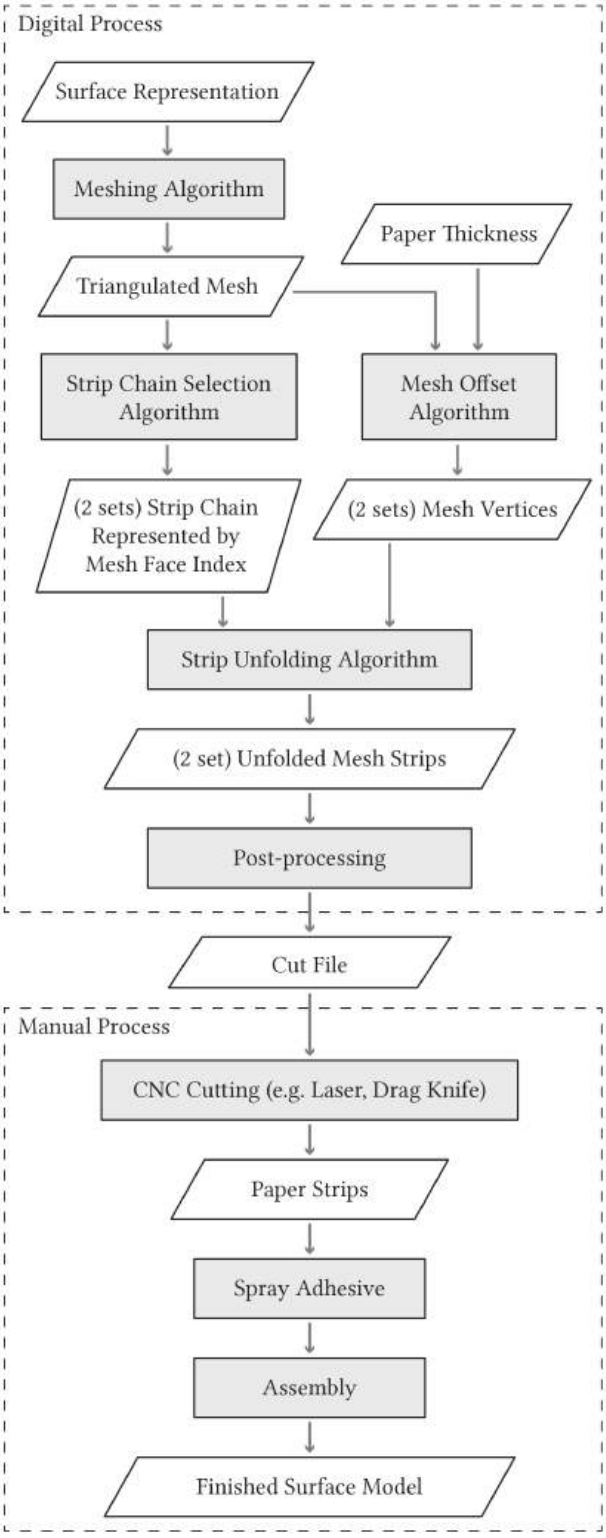

Figure 3: Overview of the computation and manual assembly workflow of the proposed "Double Shell" method.

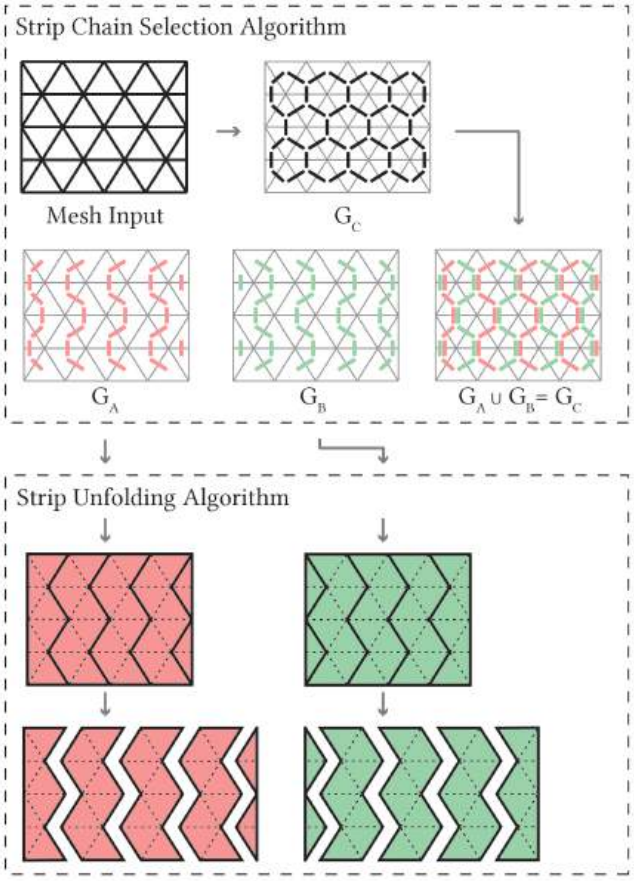

Figure 4: Computational workflow of strip chain selection and unfolding.

Alternatively, any orientable planar mesh input can be used. We present a simple algorithm based on the work of Nejur and Steinfeld [2016]. They have demonstrated the use of dual graph as an important technique for mesh segmentation in the context of computer-aided architectural design. We extend their strip selection method to create two sets of strips on any mesh with arbitrary topology.

3.2 Strip Chain Selection

The strip chain selection criteria for this method are similar to existing solutions surveyed by Nejur and Steinfeld [2016] to maximize chain lengths and avoid self-overlapping. However, our method additionally requires the generation of a second set of strips that, when two sets are combined, completes all the edge connections in the original mesh. The problem can be analysed as follow:

A connectivity graph $G_C = (V_C, E_C)$ can be generated by computing the weak dual graph from the input mesh (Figure 4). V_C represent the mesh faces in the input mesh and E_C represent mesh-face-to-mesh-face connections (i.e. edge joints). The solution to the two sets of strip chains should follow the following criteria:

(1) their connectivity graph (G_A and G_B) is a subgraph of G_C.
(2) they must contain all the mesh faces from the input mesh: $V_A = V_B = V_C$
(3) their edges are a subset from the connectivity graph where: $E_A \subset E_C$ and $E_B \subset E_C$ (Each connected path or tree in E_A and E_B, represents one resulting strip.)
(4) all chains or trees in G_A and G_B must be an acyclic, internally vertex-disjoint path. (E_A and E_B may contain the same edges).
(5) edges of G_A and G_B creates a union set that equals to all edges of G_C such that: $E_A \cup E_B = E_C$
(6) mesh faces represented by all chains or trees in G_A and G_B must not cause self-overlap when unfolded.

Additional optimization to reduce strip chain count should be performed to minimise manual assembly time used for sorting small pieces. For example, a valid solution may contain vertices in V_A or V_B that are not connected by any edge. While these single mesh faces can be unfolded and fabricated separately from any chains, this condition may not be ideal for visual appearance or minimal strip count.

Figure 4 shows an overview of the computational workflow from a mesh input to two sets of strips. G_C is first computed from the mesh input, then G_A and G_B are derived according the above criteria. G_A and G_B are then fed to the unfolding algorithm in the next step for planar fabrication.

3.2.1 Algorithm for regular topology mesh. We have found two approach to implement the strip chain selection algorithm depending on the input mesh topology. For surfaces that originates from a rectilinear topology, such as B-spline surfaces, a regular mesh topology is usually present as a result of the meshing algorithms. A regular chaining pattern can then be applied to these meshes which produce very optimized solutions. Figure 5 shows some of the standard solutions that can be applied to regular rectangular and triangular mesh topologies. Notice many solutions features a zigzag strip pattern which allows the assembly sequence to progress strip by strip, further reducing the assembly difficulty.

3.2.2 Algorithm for arbitrary topology mesh. For mesh input with arbitrarily defined topology, we present an algorithm that aims to satisfy the mentioned constraints while minimizing the number of strips. It first creates one strip selection set $G_A = (V_A, E_A)$ based on the orange peel method described by [Nejur and Steinfeld 2016]. The unconnected edges are then used to create the second set $G_B = (V_B, E_B)$ where $V_B = V_A$, $E_B = (E_C \setminus E_A)$. This typically results in a large amount of short disjoint chains. Edges in EA are then added one-by-one back to GB to minimize the number of strips while checking for self-overlap. We found this algorithm generates satisfactory results for many triangular meshes. (Figure 6) The following is the detailed strip selection algorithm for generating G_A:

(1) Compute dual graph $G = (V, E)$ from the input mesh.
(2) Assign integer weights to each E based on the orange peel method presented by [Taubin and Rossignac 1998] implemented in Ivy [Nejur and Steinfeld 2016]. Edges along peel have weights of 0 while edges across peels have weights of 1.

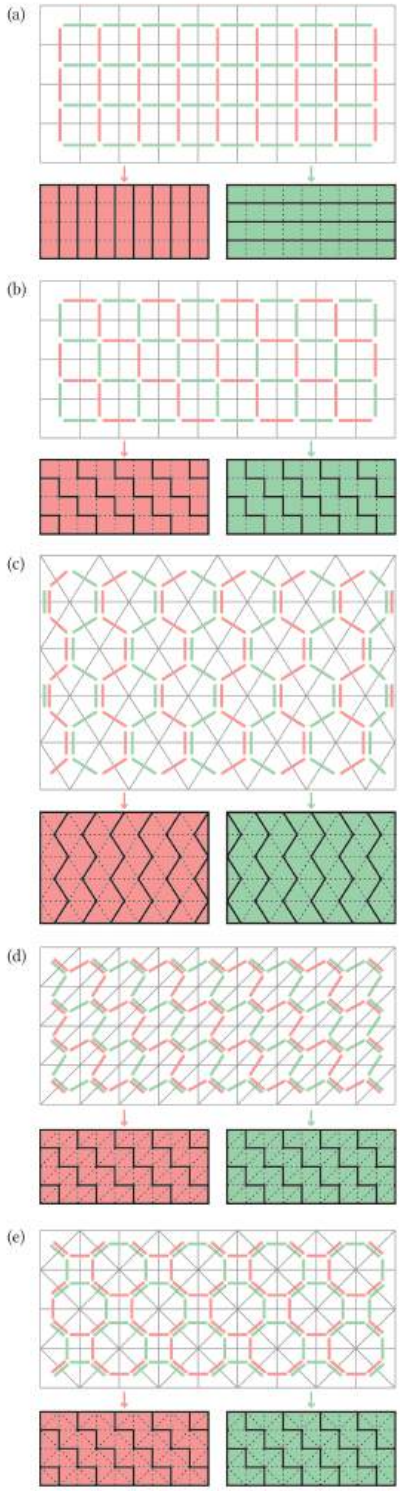

Figure 5: Standard chain selection solutions for regular mesh topology. (a), (b) two possible solutions for square grid; (c), (d) valence-6 triangular grid; (e) valence-4,8 triangular grid

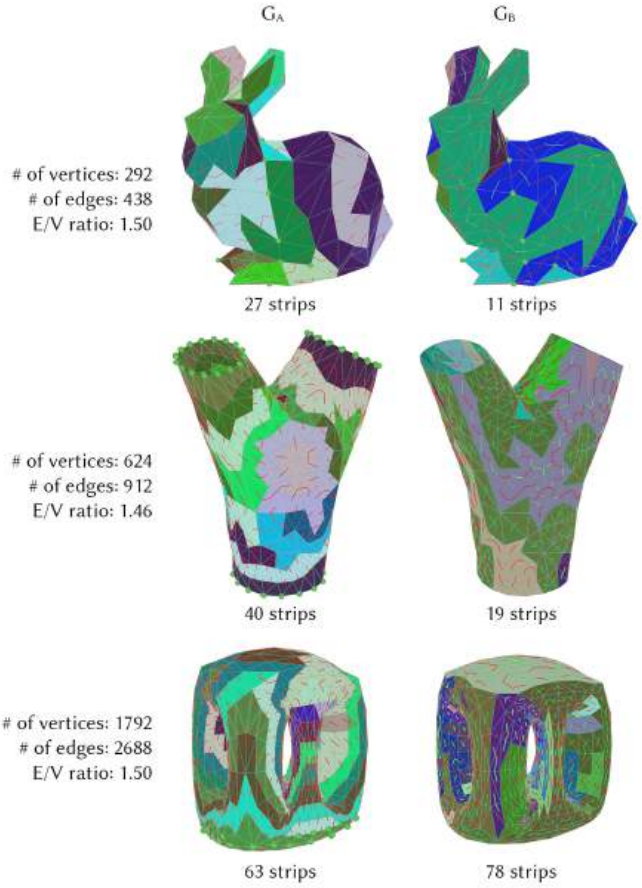

Figure 6: Chain selection result on test meshes with arbitrary topology. Top: closed mesh with low polygon count. Middle: Open mesh with three naked edges. Bottom: Closed Mesh with bridge topology. Green Dots indicate initial mesh vertices for the orange peel method. Red lines indicate unconnected edges $E_B = (E_C \setminus E_A)$ that are used to create G_B. Green lines indicate edges from E_A that are then added back to G_B to reduce strip count. All three solutions satisfy the strip selection criteria.

(3) Perform a modified Kruskal's algorithm where edges with weight 1 are ignored. (The result may not be a spanning tree)
(4) Each disjoint path is unfolded to check for self-overlap, and invalid chains are split [Nejur and Steinfeld 2017]. The resulting graph becomes G_A.

The following is the strip selection algorithm for generating G_B:

(1) Compute dual graph $G = (V, E)$ from the input mesh.
(2) Create graph $G_B = (V_B, E_B)$ where $V_B = V_A$, $E_B = (E_C \setminus E_A)$ (At this point, if all chains in G_B are acyclic and passes the self- overlap check, we can guarantee to reach a valid solution. Otherwise, we can still proceed by splitting the invalid paths, but the resulting $E_A \cup E_B$ will fall short of E_C)

(3) Examine each edge in E_A by adding each one to E_B one at a time.
   (a) If the new edge does not connect two different trees in G_B, undo the addition and proceed to next edge.
   (b) If the newly joined tree by the new edge does not pass the self-overlap check, undo the addition and proceed to next edge.
(4) The resulting graph becomes G_B.

The orange peel method is selected to generate the first set because of its tendency to create long chains that are parallel to each other. This has a positive effect in reducing the likelihood of self-overlap in the unfolded state [Nejur and Steinfeld 2017] for set A. It also produces a set of less connected edges ($E_C \setminus E_A$), for set B, which reduce the chance of an invalid solution that is described in step 2 above. Note that the choice of initial vertices for the orange peel method can affect the selection result. For meshes with naked edges, using the mesh faces with naked edge(s) as initial vertices typically generates good result. For closed surfaces, a single random point or a set of user selected points along a strip can be used as initial vertices.

3.2.3 Unconnected edges. Despite best efforts, certain mesh topology may not bear any valid solution, and some edges must remain unconnected. While this may create visible gaps and affect the appearance of the paper model, one can still choose to continue with the model as the occasional occurrence of isolated broken edges are unlikely to affect the overall structural integrity. The gaps can also be carefully repaired with glue.

The likelihood of successful selection is related to the Edge to Vertex ratio (E/ V ratio) of the input mesh. Because the goal of the strip selection criteria is to complete all E_C by means of chains in $E_A \cup E_B$, and because the maximum number of edges each acyclic chain can have is equal to the number of vertex minus one, therefor meshes with lower E/V ratio have more vertices to complete all the edges. As such, triangulated meshes are more likely to have a solution due to the lower E/V ratio (≈ 1.5) compared to meshes with quad faces (E/V ratio ≈ 2.0). Using a simple example (Figure 7), a cube with 6 quad faces that has a E/V ratio of 2.0 can be shown to have no solution that satisfy the selection criteria:

(1) A cube has 12 E_C and 6 V_C. (E/V ratio of 2.0)
(2) Because $V_A = V_B = V_C$. There are 6 V_A and 6 V_B

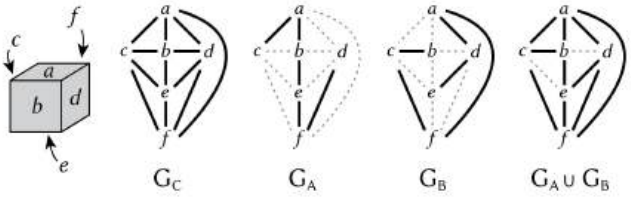

Figure 7: Diagram showing no valid solution can be found on a cube. G_C: Dual graph of a cube. G_A and G_B: Dual graph of two acyclic chains that does not share edge, each with 5 edges. $G_A \cup G_B$ showing 2 edges are missing despite best efforts.

(3) Because each vertex disjoint path can only have a maximum number of edges equals to the number of vertex minus one.
(4) Maximum number of E_A or E_B is $(6 - 1) = 5$.
(5) Maximum number of $E_A \cup E_B$ is $(2 \times 5) = 10$, which is less than the number of E_C 12.

3.3 Mesh offset

Because each set of strips are assembled on one side of the surface model, paper thickness will cause the concave side of the surface smaller than the convex side. This effect becomes noticeable when the paper thickness to edge length ratio (paper thickness / average length of all mesh edges) exceeds 0.01, misalignment may occur between the two layers if this is not compensated.

Mesh face-offsetting operations can be used to generate a new mesh whose face planes are parallel and at fixed distance from the original faces. This topic has been extensively studied [Pottmann and Wallner 2008; Wang and Liu 2010] because of the recent bloom of free form architectural construction. It should be noted that no offseting scheme is perfect. Vertex offsetting does not guarantee parallel faces and edge-parallel [Ross 2015] meshes do not guarantee resulting vertices to meet at the same point. However, for the small amount of offset in our application, eiher method will create acceptable results. In particular, vertex offsetting was implemented in our demonstration.

The demonstrations presented in this paper uses a simple vertex offset algorithm by translating each vertex along their normal by a constant distance. This algorithm does not generate precise face offset, but is faster to compute. Visual confirmation of edge gaps and misalignments on empirical experiments proves that such simple offset is sufficient for cardboard thickness 0.7mm and below. Mesh A and B, corresponding to strip set G_A and G_B, are created by offsetting the input mesh by half of the paper thickness towards either sides.

3.4 Strip unfolding

Strip unfolding and the associated self-overlap check is based on a series of rotational transformation. Starting from the outermost leaf of a mesh chain, the vertex of all remaining faces are rotated along the shared edge such that the current face and the next face are coplanar. The process repeats on the next face until all remaining faces are coplanar, the planar strip is then relocated onto the XY plane for layout. Note that this operation can only operate on planar faces. The self-overlap test is then performed by calculating if any unfolded faces overlaps with any other faces. Both set of strips are arranged to face the same direction for laser cutting (Figure 8).

3.5 Post processing for Digital Fabrication

The final step to convert the unfolded mesh strips for digital fabrication is to extract the naked edges as cut lines and shared edges as folding lines. It is also possible to introduce other geometries to the mesh faces such as face openings, alignment curves and surface trim lines.

It may be beneficial to introduce a small break along the cut lines such that the strips are retained with the material after cutting. This can speed up the glue spraying or rolling process. Identification tags can be added to the cut file (with corresponding tags on the

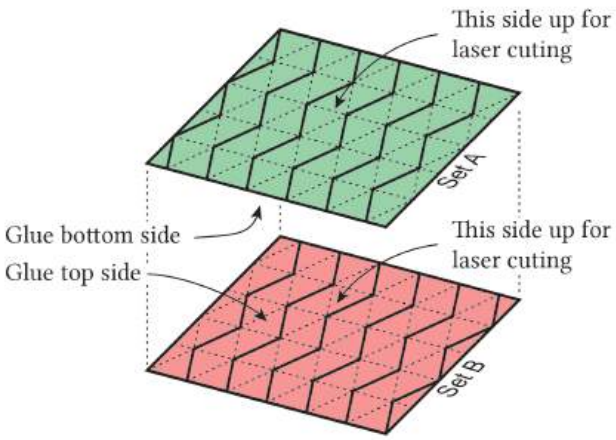

Figure 8: Diagram showing the face orientation of the strips for laser cutting and gluing.

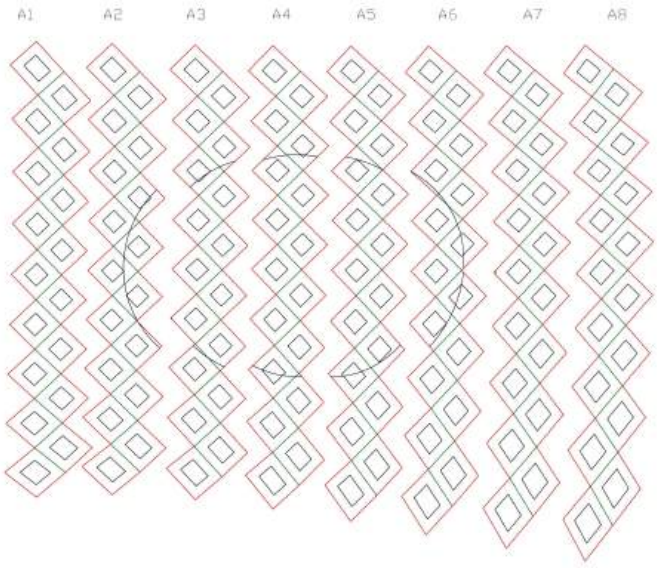

Figure 9: Part of the laser cutting file used to produce model shown in figure 1. Strips are nested, unfolded with the addition of identification tag, face opening and trim lines. Red and black lines represent through-cut and green lines represent engraving-cut. The trim lines reproduce the boundary of the trimmed NURBS surface.

3D model) to assist assembly. Nesting operations (Figure 9) can be used to layout the strips to reduce material waste.

A laser cutter is used in our demonstrations because of its capability in cutting delicate geometry on a wide range of paper thickness. Alternatively, a drag knife cutter can also be used for its advantage of producing clean edges without burn marks.

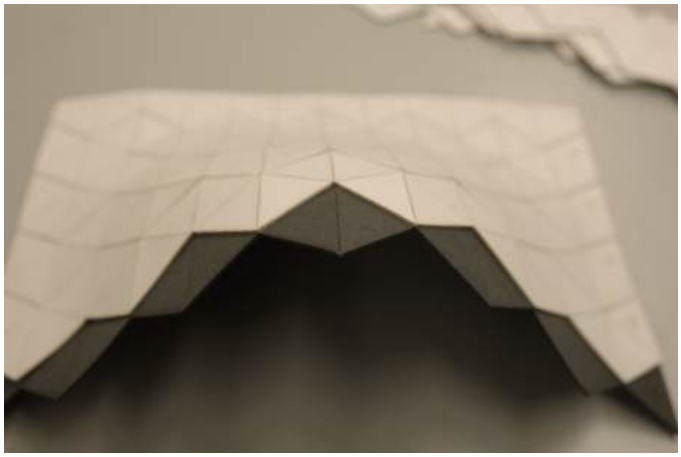

Figure 10: Photo during strip assembly. Top and bottom layer made with white and black cardboard respectively.

Figure 11: Assembled surface with rigid perimeter support.

3.6 Gluing and assembly

Spray-on contact adhesive (3M Super 77^{TM} Multipurpose Spray Adhesive) is applied on the bottom side of set A strips, and the top side of set B strips (Figure 8), followed by the waiting time indicated on the instructions. Glue can be sprayed to multiple strips in a batch to save time. Alternatively, the strips can be cut from sticky paper with peel off backing or water activated glue to eliminate the need of spraying. The zigzag strips are then assembled one at a time, starting from one edge of the surface, to complete the model. (Figure 10) It may be necessary to pre-fold the strips into an approximate shape before sticking them together.

Shifting may occur between the two layers if the model is carelessly assembled. Visual alignment of the strip edges to the etched folding lines on the other side can reduce shifting. When using a zigzag strip pattern, an alternative assembly sequence is to first stick pairs of consecutive strips together (one from set A and B), then assemble the pairs into a surface. This can avoid shifting error to accumulate as the assembly progress.

Figure 12: Hyperbolic paraboloid models of different tessellation density made by the traditional "Gluing Tab" method (front row) and the proposed "Double Shell" method (back row).

Depending on the amount of non-zero Gaussian curvature present on the surface, the resulting surface may not be rigid enough to maintain its shape. Rigid support at the perimeter (Figure 11) or stiffening plates may be added to stiffen the surface.

4 RESULTS

4.1 Assembly effort

The main improvement offered by the "Double Shell" method is the increased assembly speed over the traditional "Gluing Tab" method. We have performed an empirical study of fabricating multiple 200mm × 200mm hyperbolic paraboloid using 0.38mm thick paper. An Epilog Fusion laser cutter is used to cut the paper. An architectural student, skillful in both methods, performs the assembly with high priority for the resulting visual appearance. It provides a rough comparison of the cutting and assembly time between the two methods. The smooth surface is modelled in Rhino 5 and tessellated by a triangular tiling pattern, three different resolutions are used (Figure 12). Table 1 shows the reduction in assembly time. The trend shows a higher percentage of time reduction as the number of triangles increase.

The zig-zag strip chain selection algorithm, the mesh vertex offset algorithm and the mentioned unfolding algorithm were implemented in Grasshopper v1.0 (a plugin for Rhino 5).

4.2 Appearance

The second improvement of the "Double Shell" method over traditional "Gluing Tab" is the ease of producing a model that is visually appealing and visually identical on both sides. Figure 14 shows the front and back side of both methods for comparison. By eliminating the need for gluing tabs, the "Double Shell" models show only the triangular tessellation grid pattern while the tabs are clearly visible on the back side of the traditional method. If strip set B were to be laser cut in a flipped position, it would further reduce the difference in appearance due to laser charring on the back side of the paper.

The "Double shell" method also has the advantage of avoiding a stepped surface artefact when using thicker paper. This is because the "Double Shell" has a constant thickness of two sheets of paper, while "Gluing tab" surfaces varies between one layer and two layers of thickness (Figure 13).

Table 1: Cutting and assembly time of models shown in figure 10

Number of triangle faces (count)		110	342	930
Average edge length (mm)		34.8	19.8	12.0
Number of edge to edge connections (count)		50	162	450
Gluing Tab Method	Cutting Time (min)	4.3	5.5	10.8
	Assembly Time (min)	25	52	120
	Total Time (min)	**29.3**	**57.5**	**130.8**
Double Shell Method	Cutting Time (min)	6.7 (+55%)	8.2 (+49%)	16.0 (+48%)
	Assembly Time (min)	16 (-24%)	35 (-33%)	790 (-34%)
	Total Time (min)	**22.7 (-23%)**	**43.2 (-25%)**	**95.0 (-27%)**

4.3 Large models

The proposed method can be used to create large surfaces with large curvatures. Figure 15 shows a 400mm × 800mm × 150mm surface that is otherwise too big for 3D printing. It contains 1380 triangular faces with average edge length 24.2mm. Each side is constructed with 35 strips of 0.38mm thick paper. The non-zero Gaussian curvature of the surface provided sufficient rigidity for maintaining its own shape.

4.4 Paper thickness

The choice of paper thickness is not limited by the shell doubling or the imprecision caused by surface offset, but rather the flexibility of the paper to be fold at the creases without cracking. Depending on the stiffness and rigidity required, paper thickness ranging from 0.15mm to 0.7mm can be used. It should be noted that thickness below 0.20mm is difficult to be cut by laser systems while larger than 0.5mm may not bend properly at sharp fold.

To verify the effect of different offset distance for thicker material, three curved models (200mm × 300mm × 90mm) (Figure 16) are

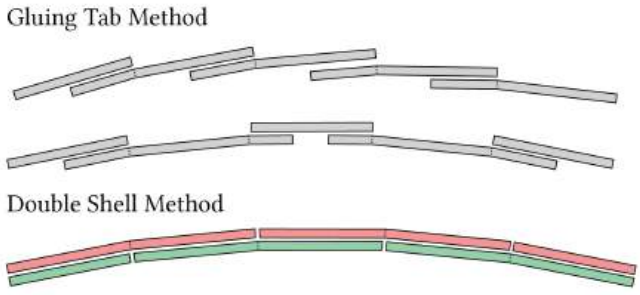

Figure 13: Diagram showing the stepped effect along a section of a "Gluing Tab" model versus the constant thickness in a "Double Shell" model.

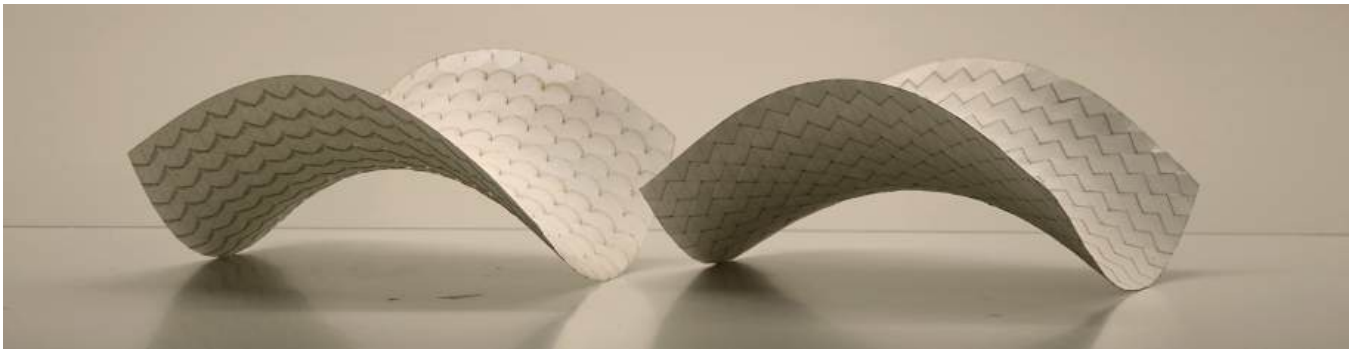

Figure 14: Two hyperbolic paraboloid models with identical mesh input, made by the traditional "Gluing Tab" method and the proposed "Double Shell" method. Photo showing top and bottom surface simultaneously.

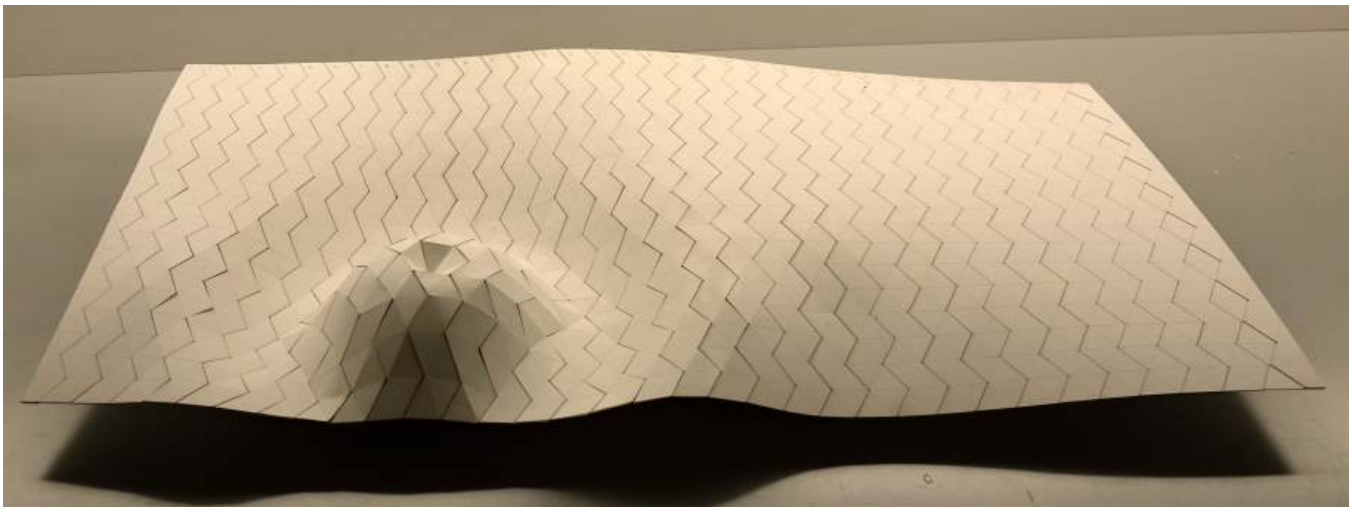

Figure 15: Large surface model of a diminishing sine wave. 400mm × 800mm × 150mm.

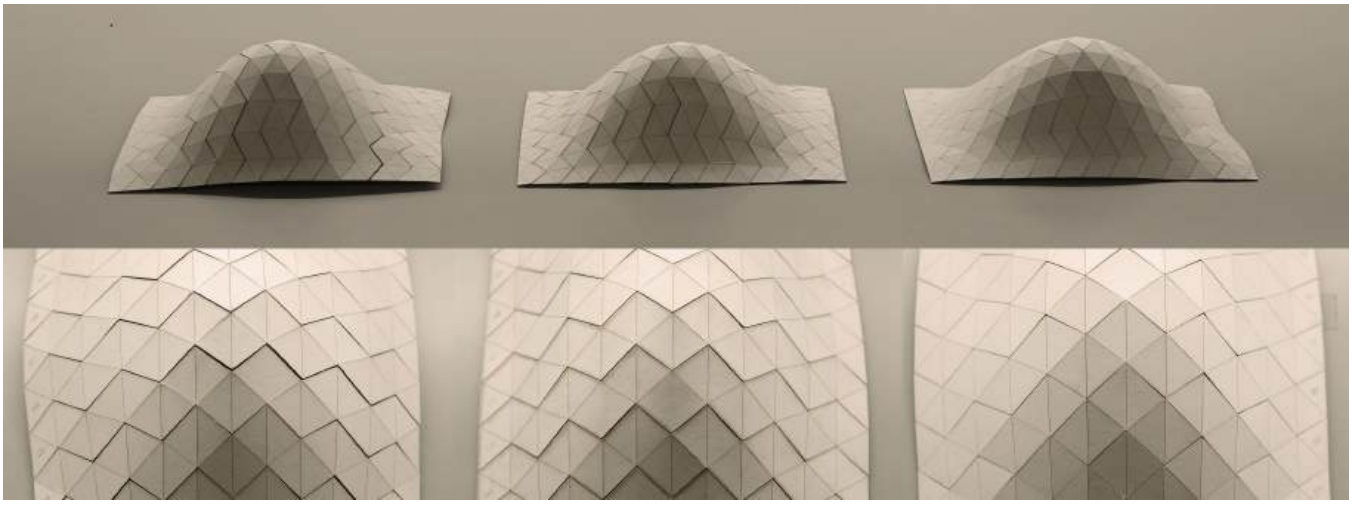

Figure 16: Curved surface model with identical mesh input, different amount of mesh offset.(left) 0.0mm, (mid) 0.5mm, (right) 0.7mm.

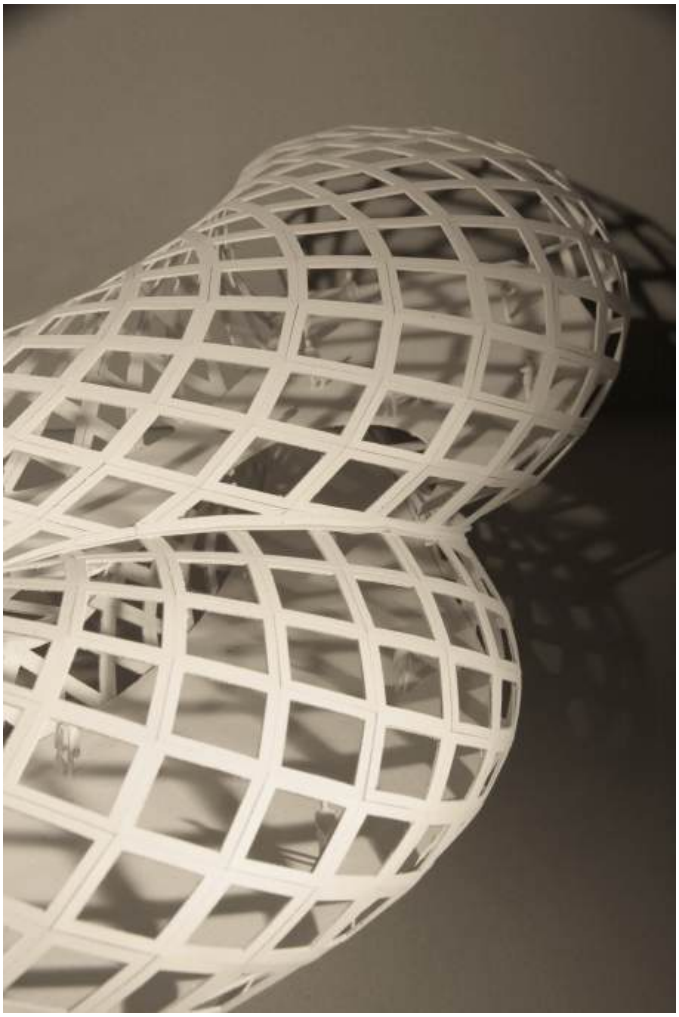

Figure 17: Photo of two NURBS surface models with boundary trim curves. Openings are added to each face of the model.

constructed with 0.7mm thick cardboard. The models originate from an identical surface input and tessellation, differ only by the amount of mesh offset. Three different offset amount were tested using a simple vertex offset, 0.0mm, 0.5mm, 0.7mm. (This value represent paper thickness compensation, actual offset of each side is half of this amount) The result shows a decrease in layer misalignment and gaps between strips as the offset distance approach the same amount as the paper thickness (0.7mm). Assembly process was also found to be easier without the constant need to force the paper into correct alignment.

4.5 Variations

Curves on the input surface can be projected onto the mesh model and unfolded together with the strips. This allows trimmed NURBS surfaces to be fabricated by projecting the trim lines on the unfolded strips. The tessellation grid can also be incorporated strategically into the design of the surface to create openings. Figure 17 shows a building model designed with two intersecting tubes, the tessellation grid represents the structural system; the openings on each face, represent windows.

5 CONCLUSION AND FUTURE WORK

This paper demonstrated a double shell construction method to create non-developable mesh models. This method allows anyone with a laser cutter or drag knife cutter to rapidly create mesh models that are easy to assemble and aesthetically clean on both sides.

Compared to the traditional method of using gluing tabs, the double shell method creates paper models that are constant in thickness and without stepping artefacts. The removal of the typically trapezoidal gluing tabs allows both sides of the surface to look similar and free from visual distractions. The speed of assembly is increased due to the use of spray-on contact adhesive, which was previously not possible with gluing tabs. Bonding between faces are instant and there is no chance of glue oozing from the joints.

Future demonstrations will aim to apply the method to construct non-developable surface models of buildings and ships, and investigate how other building elements such as floor plates, columns and structural support can be connected with the model. Paper with peel-off backing will also be tested. 3D scans of the constructed models can also help to verify the precision of the method.

ACKNOWLEDGMENTS

The author would like to thank CROLLA, Kristof [1] for supporting the project while the author was studying in his design studio in The University of Hong Kong; MO, Yee Lam[2] for her assistance in the strip selection algorithm; and CHEUNG, King Man Zoe[3] for her assistance in constructing the paper models.

The author would also like to thank the anonymous reviewers for their valuable comments and helpful suggestions.

REFERENCES

Mark Burry. 2016. Antoni GaudÃŋ and Frei Otto: Essential Precursors to the Parametricism Manifesto. *Architectural Design* 86, 2 (2016), 30–35. https://doi.org/10.1002/ad.2021 arXiv:https://onlinelibrary.wiley.com/doi/pdf/10.1002/ad.2021

Suryansh Chandra, Axel Körner, Antiopi Koronaki, Rachelle Spiteri, Radhika Amin, Samidha Kowli, and Michael Weinstock. 2015. Computing Curved-folded Tessellations Through Straight-folding Approximation. In *Proceedings of the Symposium on Simulation for Architecture & Urban Design (SimAUD '15)*. Society for Computer Simulation International, San Diego, CA, USA, 152–159. http://dl.acm.org/citation.cfm?id=2873021.2873042

ABNET CORP. 2017. Pepakura Designer. Retrieved Jan 27, 2017 from http://www.e-cardmodel.com/pepakura-en/

Gershon Elber. 1995. Model fabrication using surface layout projection. *Computer-Aided Design* 27, 4 (1995), 283 – 291. https://doi.org/10.1016/0010-4485(95)91138-B

Michael Garland and Paul S. Heckbert. 1997. Surface Simplification Using Quadric Error Metrics. In *Proceedings of the 24th Annual Conference on Computer Graphics and Interactive Techniques (SIGGRAPH '97)*. ACM Press/Addison-Wesley Publishing Co., New York, NY, USA, 209–216. https://doi.org/10.1145/258734.258849

F. Gonzalez-Quintial, J. Barrallo, and A. Artiz-Elkarte. 2015. Freeform surfaces adaptation using developable strips and planar quadrilateral facets. *Journal of Facade Design and Engineering* 3, 1 (2015), 59–70. https://doi.org/10.3233/FDE-150033

Axel Kilian. 2003. Fabrication of Partially Double-Curved Surfaces out of Flat Sheet Material Through a 3D Puzzle Approach.. In *Crossroads of Digital Discourse: Proceedings of the 2003 Annual Conference of the Association for Computer Aided Design in Architecture (ACADIA)*. ACADIA, Indianapolis, 75–83.

[1] now at The Chinese University of Hong Kong
[2] Hang Seng Management College, Hong Kong
[3] The University of Hong Kong

Axel Kilian. undated. Embodied Intelligence. Final Project. Using Genetic Algorithms To Generate Developable Strips From Free Formed Surfaces. http://www.designexplorer.net/ Last accessed 31 March 2017.

D López López, T Van Mele, and P Block. 2016. Tile vaulting in the 21 st century. *Informes de la ConstrucciÂşn* 68, 544 (2016), 162. https://doi.org/10.3989/ic.15.169.m15

Daniel Lordick. 2009. Intuitive Design and Meshing of Non-Developable Ruled Surfaces. In *Proceedings of the Design Modelling Symposium Berlin 2009*. UniversitÃđt der KÃijnste Berlin, 249–260.

Jun Mitani and Hiromasa Suzuki. 2004. Making Papercraft Toys from Meshes Using Strip-based Approximate Unfolding. *ACM Trans. Graph.* 23, 3 (Aug. 2004), 259–263. https://doi.org/10.1145/1015706.1015711

Andrei Nejur and Kyle Steinfeld. 2016. Ivy: Bringing a Weighted-Mesh Representations to Bear on Generative Architectural Design Applications. In *Proceedings of the 36th Annual Conference of the Association for Computer Aided Design in Architecture (ACADIA)*. ACADIA 2016: POSTHUMAN FRONTIERS: Data, Designers, and Cognitive Machines, Ann Arbor, 140–151. http://papers.cumincad.org/cgi-bin/works/Show?acadia16_140

Andrei Nejur and Kyle Steinfeld. 2017. Ivy: Progress in Developing Practical Applications for a Weighted-Mesh Representation for Use in Generative Architectural Design. In *Proceedings of the 37th Annual Conference of the Association for Computer Aided Design in Architecture (ACADIA)*. ACADIA 2017: DISCIPLINES & DISRUPTION, Cambridge, MA, 446–455. http://papers.cumincad.org/cgi-bin/works/Show?acadia17_446

Helmut Pottmann and Gerald Farin. 1995. Developable Rational Be&Acute;Zier and B-spline Surfaces. *Comput. Aided Geom. Des.* 12, 5 (Aug. 1995), 513–531. https://doi.org/10.1016/0167-8396(94)00031-M

Helmut Pottmann and Johannes Wallner. 2008. The focal geometry of circular and conical meshes. *Advances in Computational Mathematics* 29, 3 (01 Oct 2008), 249–268. https://doi.org/10.1007/s10444-007-9045-4

Daniel Ross, Elissa; Hambleton. 2015. Exact Face-Offsetting for Polygonal Meshes. In *Proceedings of the 35th Annual Conference of the Association for Computer Aided Design in Architecture (ACADIA)*. ACADIA 2105: Computational Ecologies: Design in the Anthropocene, Cincinnati. http://papers.cumincad.org/cgi-bin/works/Show?acadia15_203

Shapeways. 2017. PLA 3D Printing Material Information. Retrieved Dec 28, 2017 from https://www.shapeways.com/materials/pla

J. Stewart. 2010. *Single variable calculus*. Brooks/Cole Cengage Learning, Australia. ii pages.

Masahito Takezawa, Takuma Imai, Kentaro Shida, and Takashi Maekawa. 2016. Fabrication of Freeform Objects by Principal Strips. *ACM Trans. Graph.* 35, 6, Article 225 (Nov. 2016), 12 pages. https://doi.org/10.1145/2980179.2982406

Gabriel Taubin and Jarek Rossignac. 1998. Geometric Compression Through Topological Surgery. *ACM Trans. Graph.* 17, 2 (April 1998), 84–115. https://doi.org/10.1145/274363.274365

Wenping Wang and Yang Liu. 2010. A Note on Planar Hexagonal Meshes. In *Nonlinear Computational Geometry*, Ioannis Z. Emiris, Frank Sottile, and Thorsten Theobald (Eds.). Springer New York, New York, NY, 221–233. https://doi.org/10.1007/978-1-4419-0999-2_9